Least-squares reverse time migration incorporating prismatic waves

Jizhong Yang[1, 2], Yuzhu Liu[1], Liangguo Dong[1], Yunyue Elita Li[2], and Arthur Cheng[2]*
[1] State Key Laboratory of Marine Geology, Tongji University
[2] Department of Civil and Environmental Engineering, National University of Singapore

Summary

Least-squares reverse time migration (LSRTM) of primary waves has the potential to enhance the spatial resolution, balance the amplitudes, and reduce the migration artifacts compared to the standard reverse time migration (RTM). However, it cannot delineate the steep structures, such as the vertical or nearly vertical faults and salt flanks, as the primary waves do not illuminate these structures. The prismatic waves, however, can go through these structures to some extent. Migration of the prismatic waves may help to enhance the imaging of them. In this study, we propose a LSRTM scheme that can incorporate the prismatic waves together with the primary waves for subsurface imaging, through which the steep structures can be delineated. The numerical examples show the feasibility of our method.

Introduction

Migration of the primary waves only cannot provide well-defined images of steep structures, such as the vertical or nearly vertical faults and salt flanks, because the illuminations of the single-scattered energy to these areas are insufficiently recorded on the surface. Turning waves, if strong gradient exists in the velocity model, can make a significant contribution for migrating these events (Hale et al., 1992; Xu and Jin, 2006).

Prismatic waves, also known as duplex waves or doubly-scattered waves, can be migrated for delineation of steep structures, if the turning waves are not extant due to the absence of a strong velocity gradient or a limited recording aperture. Marmalyevskyy et al. (2005) migrated the prismatic waves by a Kirchhoff-based method for salt flank delineation with sub-horizontal reflection boundaries specified from the previous migration images. Jin el al. (2006) migrated the prismatic waves using the one-return one-way wave-equation method. An iterative method was proposed by Malcolm et al. (2009) to progressively incorporate migration of prismatic waves and multiples with a modified one-way wave equation migration method, where each phase was isolated by a data fitting process. Li et al. (2011) improved the traditional reverse-time migration and proposed a prismatic imaging process for complex salt dome structures. Dai and Schuster (2013) proposed the prismatic RTM method, which does not need to extract the horizontal reflection layers in advance.

Aldawood et al. (2015) proposed a Kirchhoff-based linearized inversion framework for imaging of doubly scattered internal multiples, which are essentially the prismatic waves discussed here. The least-squares image, based on the single-scattering assumption, is used as a constraint to linearize the forward modeling and adjoint operators of doubly scattered energy.

In this study, we propose a LSRTM scheme that can jointly migrate the primary and prismatic waves. We will give a detailed description of the implementation procedure. The numerical examples based on a simple “L” model and a salt-like model demonstrate the effectiveness of our method.

Methodology

In this section, we first briefly review the methodology involved in conventional LSRTM, which is mainly focused on migration of primary waves. Then we define the imaging condition for migration of prismatic waves. After that, we describe the theory for joint LSRTM of primary and prismatic waves.

Conventional least-squares reverse time migration

Under the Born approximation of the constant-density acoustic wave equation, the single-scattered seismic data recorded by a receiver at $\boldsymbol{x}_r$ emitted by a source at $\boldsymbol{x}_s$ can be linearly expressed as:

$$d\left(\boldsymbol{x}_r,\boldsymbol{x}_s,\omega\right)=\omega^2\sum_{\boldsymbol{x}} f_s\left(\omega\right)\boldsymbol{G}\left(\boldsymbol{x},\boldsymbol{x}_s,\omega\right)\boldsymbol{G}\left(\boldsymbol{x}_r,\boldsymbol{x},\omega\right)\boldsymbol{m}\left(\boldsymbol{x}\right), \quad (1)$$

where ω is the angular frequency, $f_s\left(\omega\right)$ is the source signature, $\boldsymbol{m}\left(\boldsymbol{x}\right)$ denotes the reflectivity (a perturbation to the background velocity model) at imaging point $\boldsymbol{x}$ in the subsurface. $\boldsymbol{G}\left(\boldsymbol{x},\boldsymbol{x}_s,\omega\right)$ and $\boldsymbol{G}\left(\boldsymbol{x}_r,\boldsymbol{x},\omega\right)$ are the monochromatic Green’s function from the source $\boldsymbol{x}_s$ to imaging point $\boldsymbol{x}$ and from imaging point $\boldsymbol{x}$ to the receiver $\boldsymbol{x}_r$ in the background media, respectively. For simplicity, the term ω is omitted in the following sections.

In a matrix notation, equation (1) can be expressed as:

$$\boldsymbol{d}=\boldsymbol{L}_0\boldsymbol{m}\ , \quad (2)$$

where $\boldsymbol{L}_0$ denotes the linearized forward Born modelling operator. A standard migrated image $\boldsymbol{m}_{mig}$ can be calculated by applying the adjoint of the forward Born modeling operator $\boldsymbol{L}_0^T$ to the recorded data:

$$\boldsymbol{m}_{mig}\left(\boldsymbol{x}\right)=\omega^2\sum_{s,r}\left[f_s\left(\omega\right)\boldsymbol{G}\left(\boldsymbol{x},\boldsymbol{x}_s,\omega\right)\boldsymbol{G}\left(\boldsymbol{x}_r,\boldsymbol{x},\omega\right)\right]^T d\left(\boldsymbol{x}_r,\boldsymbol{x}_s,\omega\right), \quad (3)$$

and can be expressed as a matrix-vector multiplication:

$$\boldsymbol{m}_{mig}=\boldsymbol{L}_0^T\boldsymbol{d} . \quad (4)$$

LSRTM aims to solve the reflectivity model $\boldsymbol{m}$ by minimizing the difference between the forward modeled data $\boldsymbol{L}_0\boldsymbol{m}$ and the recorded data $\boldsymbol{d}$ in a least-squares sense:

$$f\left(\boldsymbol{m}\right)=\frac{1}{2}\left\|\boldsymbol{L}_0\boldsymbol{m}-\boldsymbol{d}\right\|^2 . \quad (5)$$

The minimum of $f\left(\boldsymbol{m}\right)$ is reached when $\boldsymbol{m}$ satisfies:

$$\boldsymbol{m}=\left(\boldsymbol{L}_0^T\boldsymbol{L}_0\right)^{-1}\boldsymbol{L}_0^T\boldsymbol{d} , \quad (6)$$

or equivalently, by solving the least-squares normal equation:

$$\left(\boldsymbol{L}_0^T\boldsymbol{L}_0\right)\boldsymbol{m}=\boldsymbol{L}_0^T\boldsymbol{d} . \quad (7)$$

LSRTM under the single-scattering assumption can suppress the migration artifacts and enhances the seismic reflectors that are mainly illuminated by primaries. However, the prismatic waves and other multiples, such as the surface-related or internal multiples, are always treated as noise and cannot be properly imaged.

Imaging condition for migration of prismatic waves

Assuming that the recorded seismic data contains primary reflection waves $\boldsymbol{d}_1\left(x_r,\boldsymbol{x}_s\right)$ and the doubly scattered prismatic waves $\boldsymbol{d}_2\left(x_r,\boldsymbol{x}_s\right)$, that is

$$\boldsymbol{d}\left(x_r,\boldsymbol{x}_s\right)=\boldsymbol{d}_1\left(x_r,\boldsymbol{x}_s\right)+\boldsymbol{d}_2\left(x_r,\boldsymbol{x}_s\right) . \quad (8)$$

The reflectors are embedded in the migration velocity for generation of reflected waves. In this case, the Green's functions in equation (3) can be decomposed as:

$$\boldsymbol{G}\left(\boldsymbol{x},\boldsymbol{x}_s\right)=\boldsymbol{G}_0\left(\boldsymbol{x},\boldsymbol{x}_s\right)+\boldsymbol{G}_1\left(\boldsymbol{x},\boldsymbol{x}_s\right), \quad (9)$$

and

$$\boldsymbol{G}\left(\boldsymbol{x},\boldsymbol{x}_r\right)=\boldsymbol{G}_0\left(\boldsymbol{x},\boldsymbol{x}_r\right)+\boldsymbol{G}_1\left(\boldsymbol{x},\boldsymbol{x}_r\right), \quad (10)$$

in which $\boldsymbol{G}_0$ and $\boldsymbol{G}_1$ are the background and back-scattered wavefields, respectively.

The migrated image in equation (3) can then be described as:

$$\begin{aligned}\boldsymbol{m}_{mig}\left(\boldsymbol{x}\right)&=\omega^2\sum_{\boldsymbol{x}} \begin{matrix} f_s^T\left[\boldsymbol{G}_0^T\left(\boldsymbol{x},\boldsymbol{x}_s\right)+\boldsymbol{G}_1^T\left(\boldsymbol{x},\boldsymbol{x}_s\right)\right] \\ \left[\boldsymbol{G}_0^T\left(\boldsymbol{x},\boldsymbol{x}_r\right)+\boldsymbol{G}_1^T\left(\boldsymbol{x},\boldsymbol{x}_r\right)\right] \\ \left[d_1\left(\boldsymbol{x}_r,\boldsymbol{x}_s\right)+d_2\left(\boldsymbol{x}_r,\boldsymbol{x}_s\right)\right]\end{matrix} && (11)\\
&=\omega^2\sum_{\boldsymbol{x}} f_s^T\boldsymbol{G}_0^T\left(\boldsymbol{x},\boldsymbol{x}_s\right)\boldsymbol{G}_0^T\left(\boldsymbol{x},\boldsymbol{x}_r\right)d_1\left(\boldsymbol{x}_r,\boldsymbol{x}_s\right) && (12)\\
&+\omega^2\sum_{\boldsymbol{x}} f_s^T\boldsymbol{G}_0^T\left(\boldsymbol{x},\boldsymbol{x}_s\right)\boldsymbol{G}_0^T\left(\boldsymbol{x},\boldsymbol{x}_r\right)d_2\left(\boldsymbol{x}_r,\boldsymbol{x}_s\right) && (13)\\
&+\omega^2\sum_{\boldsymbol{x}} f_s^T\boldsymbol{G}_0^T\left(\boldsymbol{x},\boldsymbol{x}_s\right)\boldsymbol{G}_1^T\left(\boldsymbol{x},\boldsymbol{x}_r\right)d_1\left(\boldsymbol{x}_r,\boldsymbol{x}_s\right) && (14)\\
&+\omega^2\sum_{\boldsymbol{x}} f_s^T\boldsymbol{G}_1^T\left(\boldsymbol{x},\boldsymbol{x}_s\right)\boldsymbol{G}_0^T\left(\boldsymbol{x},\boldsymbol{x}_r\right)d_1\left(\boldsymbol{x}_r,\boldsymbol{x}_s\right) && (15)\\
&+\omega^2\sum_{\boldsymbol{x}} f_s^T\boldsymbol{G}_0^T\left(\boldsymbol{x},\boldsymbol{x}_s\right)\boldsymbol{G}_1^T\left(\boldsymbol{x},\boldsymbol{x}_r\right)d_2\left(\boldsymbol{x}_r,\boldsymbol{x}_s\right) && (16)\\
&+\omega^2\sum_{\boldsymbol{x}} f_s^T\boldsymbol{G}_1^T\left(\boldsymbol{x},\boldsymbol{x}_s\right)\boldsymbol{G}_0^T\left(\boldsymbol{x},\boldsymbol{x}_r\right)d_2\left(\boldsymbol{x}_r,\boldsymbol{x}_s\right) && (17)\end{aligned}$$

The term in equation (12) corresponds to the migration of primary waves, and this is what we want in conventional RTM. The term in equation (13) stands for that the prismatic waves are migrated as primary waves, and it is considered as noise for conventional RTM. Summation of the terms in equation (14) and (15) is the imaging condition for down-/up- and up-/down-going waves, and this term is always treated as low-wavenumber noise in conventional RTM (Liu et al., 2011). On the contrary, although summation of the terms in equation (16) and (17) is also related with the down-/up- and up-/down-going waves imaging, it corresponds to the imaging condition for migration of prismatic waves. The omitted higher-order terms are related with higher-order multiples which are removed from the data.

Joint least-squares reverse time migration of primary and prismatic waves

As the prismatic wave imaging is closely related with the primary wave migration, we propose the following joint LSRTM objective function:

$$f\left(\boldsymbol{m}\right)=\frac{1}{2}\left\|\left(\boldsymbol{L}_0+\boldsymbol{L}_{pris}\right)\boldsymbol{m}-\boldsymbol{d}\right\|^2 . \quad (18)$$

Here, $\boldsymbol{L}_0$ denotes the forward Born modeling operator of primary waves, and $\boldsymbol{L}_{pris}$ indicates the forward Born modeling operator of prismatic waves. The relationship between the operator $\boldsymbol{L}_{pris}$ and the recorded prismatic waves $\boldsymbol{d}_2\left(x_r,\boldsymbol{x}_s\right)$ can be expressed as:

$$d_2\left(x_r,x_s\right)=\omega^2\sum_{\boldsymbol{x}} f_s\boldsymbol{G}\left(x,x_s\right)\boldsymbol{G}\left(x',x\right)\boldsymbol{G}\left(x_r,x'\right)\boldsymbol{m}_1\left(x\right)\boldsymbol{m}_2\left(x'\right), \quad (19)$$

in which $\boldsymbol{m}_1$ denotes the image of primary waves, $\boldsymbol{m}_2$ denotes the image of prismatic waves. Notice the dependency of the operator $\boldsymbol{L}_{pris}$ on $\boldsymbol{m}_1$.

Based on equation (19), the prismatic waves can be modeled as follows. First, the seismic energy is forward propagated from the source point $\boldsymbol{x}_s$ to the scattering point $\boldsymbol{x}$ and scaled by its reflectivity value $\boldsymbol{m}_1\left(\boldsymbol{x}\right)$. Then, the energy is emitted from this secondary source at $\boldsymbol{x}$ and forward propagated to the second scattering point $\boldsymbol{x}'$ and scaled by its reflectivity value $\boldsymbol{m}_2\left(\boldsymbol{x}'\right)$. Finally, the energy is further propagated from the second scattering point $\boldsymbol{x}'$ to the receiver point $\boldsymbol{x}_r$.

Minimization of the objective function (18) can be found by computing the gradient with respect to $\boldsymbol{m}$ and setting it to zero:

$$\nabla_{\boldsymbol{m}} f = \left(\boldsymbol{L}_0 + \boldsymbol{L}_{pris}\right)^T \left(\boldsymbol{L}_0 + \boldsymbol{L}_{pris}\right)\boldsymbol{m} - \left(\boldsymbol{L}_0 + \boldsymbol{L}_{pris}\right)^T \boldsymbol{d} = 0 . \quad (20)$$

Hence, the least-squares normal equation can be formulated as:

$$\left(\boldsymbol{L}_0 + \boldsymbol{L}_{pris}\right)^T \left(\boldsymbol{L}_0 + \boldsymbol{L}_{pris}\right)\boldsymbol{m} = \left(\boldsymbol{L}_0 + \boldsymbol{L}_{pris}\right)^T \boldsymbol{d} . \quad (21)$$

In this case, the Hessian operator $\boldsymbol{H}$ is defined as:

$$\boldsymbol{H} = \boldsymbol{L}_0^T \boldsymbol{L}_0 + \boldsymbol{L}_0^T \boldsymbol{L}_{pris} + \boldsymbol{L}_{pris}^T \boldsymbol{L}_0 + \boldsymbol{L}_{pris}^T \boldsymbol{L}_{pris} . \quad (22)$$

The last term $\boldsymbol{L}_{pris}^T \boldsymbol{L}_{pris}$ in equation (22) can be dropped off due to its small amplitude.

The least-squares normal equation can be solved iteratively with a conjugate gradient algorithm, as illustrated in Table 1. Instead of explicitly constructing the Hessian matrix, the Hessian-vector products are calculated at each iteration.

Table 1: A conjugate-gradient algorithm for solving $\boldsymbol{Hm} = \boldsymbol{m}_{mig}$

Given initial $\boldsymbol{m}_0$; set $\boldsymbol{r}_0 = \boldsymbol{Hm}_0 - \boldsymbol{m}_{mig}, \boldsymbol{p}_0 = -\boldsymbol{r}_0, k = 0;$
While (the convergence condition is not satisfied)
$\alpha_k = \boldsymbol{r}_k^T \boldsymbol{r}_k \big/ \boldsymbol{p}_k^T \boldsymbol{Hp}_k$, $\boldsymbol{x}_{k+1} = \boldsymbol{x}_k + \alpha_k \boldsymbol{p}_k, \ \boldsymbol{r}_{k+1} = \boldsymbol{r}_k + \alpha_k \boldsymbol{Hp}_k$, $\beta_{k+1} = \boldsymbol{r}_{k+1}^T \boldsymbol{r}_{k+1} \big/ \boldsymbol{r}_k^T \boldsymbol{r}_k , \ \boldsymbol{p}_{k+1} = -\boldsymbol{r}_{k+1} + \beta_{k+1} \boldsymbol{p}_k$, $k = k + 1$,
End while

Explicitly writing out the Hessian-vector product $\boldsymbol{Hp}_k$ as:

$$\boldsymbol{L}_0^T \boldsymbol{L}_0 \boldsymbol{p}_k + \boldsymbol{L}_0^T \boldsymbol{L}_{pris} \boldsymbol{p}_k + \boldsymbol{L}_{pris}^T \boldsymbol{L}_0 \boldsymbol{p}_k , \quad (23)$$

the first term $\boldsymbol{L}_0^T \boldsymbol{L}_0 \boldsymbol{p}_k$ denotes the migration of the forward Born modeled data $\boldsymbol{L}_0 \boldsymbol{p}_k$, which is the same as in conventional LSRTM. The second term $\boldsymbol{L}_0^T \boldsymbol{L}_{pris} \boldsymbol{p}_k$ stands for the cross-correlation of the source-side background waves with the receiver-side back-scattered waves, as indicated in equation (16). The third term represents the cross-correlation of the receiver-side background waves with the source-side back-scattered waves, as indicated in equation (17). However, the prediction of prismatic waves is not straightforward. The recorded seismic data can be used to approximate the prismatic waves, and another way is to subtract the Born modeled data based on the LSRTM image of primary waves from the recorded data.

Numerical Examples

To show the feasibility of our method, we first apply it to a simple "L" model as shown in Figure 1a. The model has a finite difference grid dimension of 201×151, with the grid interval of 10 m. The acquisition system consists of a line of 49 sources and recorded by a coincident line of 201 receivers, with a shot interval of 40m and a receiver spacing of 10 m. The sources and receivers are on the surface, with the first source located at 40 m in distance and the first receiver lies on 0 m in distance. The source time function is a Ricker wavelet with a peak frequency of 30 Hz. The recording time is 3.0 s with the time interval of 1 ms. The migration velocity model (Figure 1b) is a constant background velocity model. Figure 2a shows the RTM image, and Figure 2b shows the conventional LSRTM image. The LSRTM provides better images than RTM in terms of better amplitude balance and higher spatial resolution. However, the vertical structures are invisible in both the LSRTM and RTM images. Figure 3a depicts the image of joint LSRTM of primary and prismatic waves, in which the recorded seismic data are directly used instead of prismatic wave for receiver-side back-propagation. The vertical structure is partially resolved. However, the inversion becomes unstable after more than 15 iterations. Then the separated prismatic waves, which are obtained by subtracting the Born modeled data based on the conventional LSRTM image as shown in Figure 2b from the recorded data, are employed for receiver-side backpropagation. The joint LSRTM image is displayed in Figure 3b. It is obvious that the imaging of the vertical structure is enhanced. Figure 4 shows seismogram of the recorded data, the data residual after conventional LSRTM, the data residual after the joint LSRTM using the recorded data as prismatic waves, and the data residual after the joint LSRTM using the approximately separated prismatic waves for the 24th shot. It is evident that, after conventional LSRTM, the primary waves are well fitted, and the data residuals are mainly prismatic waves. After the joint LSRTM using the recorded data as prismatic waves, the prismatic waves are weakly predicted. However, after joint LSRTM using the approximately separated prismatic waves, the data residuals on prismatic waves become relatively weak than the other two.

We then apply the proposed method to a salt-like model shown in Figure 5a. The model dimensions are of 401×151, with 10 m grid intervals. There are 79 shots evenly spaced at 50 m shot intervals, and each shot is recorded with 401 receivers evenly distributed at 10 m receiver spacing. The sources and receivers are on the surface, with the first source and receiver located at distances of 50 and 0 m, respectively. The source time function is a Ricker wavelet with a peak frequency of 30 Hz. The recording time is 2.5 s, with a time interval of 0.5 ms. The migration velocity model only contains the salt body as shown in Figure 5b. Figure 6a and 6b show the conventional RTM and LSRTM images, in which the salt flanks are not well delineated, although the LSRTM provides better performance than RTM with balanced amplitudes, and enhanced spatial resolution. The joint LSRTM image with prismatic data separated is shown in Figure 5c, in which the salt flanks are well depicted.

Conclusions

We have proposed a LSRTM scheme for joint migration of primary and prismatic waves. Our method maintains the advantage of the conventional LSRTM compared to the standard RTM, that is to provide images with better amplitude balance, higher spatial resolution, and reduced migration artifacts. It also has the ability to delineate the steep structures, such as the vertical or nearly vertical faults, and salt flanks, where the conventional LSRTM fails. The numerical examples have demonstrated the efficacy of our method. We have illustrated that the recorded data may be used as the prismatic waves for receiver-side backpropagation. However, the convergence and stability may be jeopardized by the crosstalk. To provide the most accurate results, one needs to separate the prismatic waves and the primary waves in the recorded data. The future work will focus on more realistic velocity models and field data applications.

Acknowledgments

We would like to thank for the financial supports of the National Natural Science Foundation of China (Grant numbers: 41474034, 41674115, and 41630964), the Fundamental Research Funds for the Central Universities (Grant number: 1350219162), the Self-determined Project of the State Key Laboratory of Marine Geology in China (Grant number: MG20160202), and the EDB Petroleum Engineering Professorship. Dr. Yunyue Elita Li and Dr. Jizhong Yang also acknowledge the founding of MOE Tier-1 Grant R-302-000-165-133.

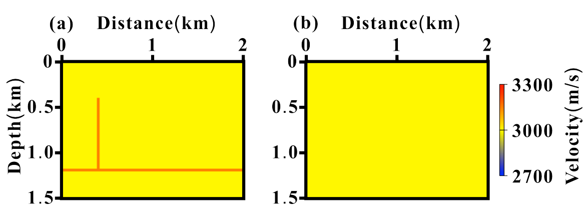

Figure 1: The “L” model for migration: (a) true velocity model, (b) migration velocity model.

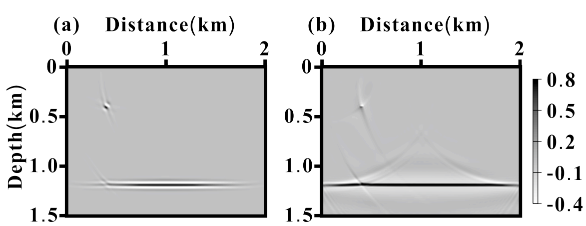

Figure 2: (a) the RTM image, (b) the conventional LSRTM image.

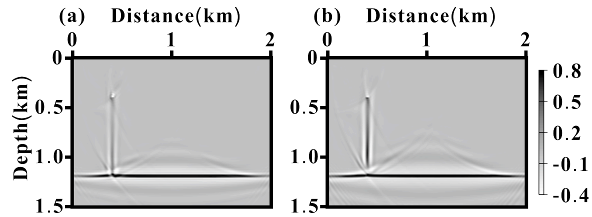

Figure 3: (a) the joint LSRTM image with the recorded seismic data injected for the receiver-side backpropagation, (b) the joint LSRTM image with the separated prismatic waves injected for the receiver-side backpropagation.

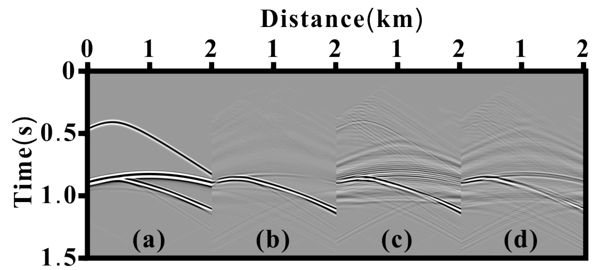

Figure 4: the seismogram of (a) the recorded data, (b) the data residual after the conventional LSRTM, (c) the data residual after the joint LSRTM using the recorded data as prismatic waves, and (d) the data residual after the joint LSRTM using the approximately separated prismatic waves for the 24th shot.

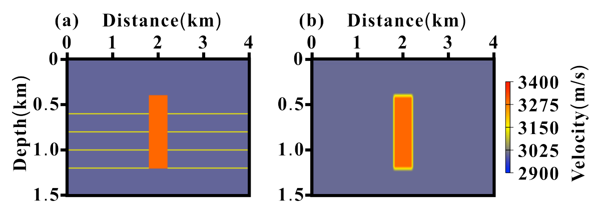

Figure 5: The salt-like model for migration: (a) true velocity model, (b) migration velocity model.

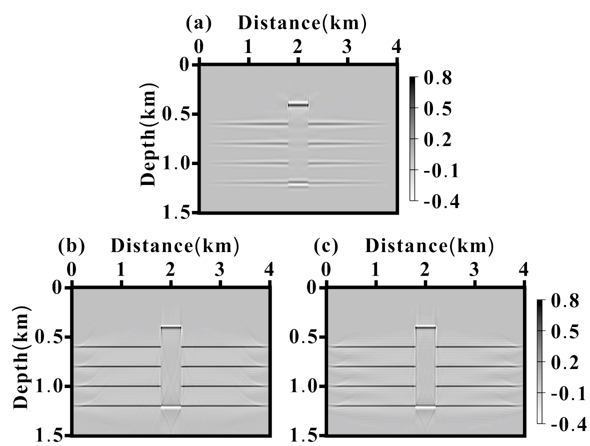

Figure 6: (a) the RTM image, (b) the conventional LSRTM image, (c) the joint LSRTM image.

REFERENCE CHANGE: Reference lists **will not** be included at the end of the expanded abstract, but should be prepared separately and entered during the submission process in the online form.

Aldawood, A., I. Hoteit, M. Zuberi, G. Turkiyyah, and T. AlKhalifah, 2015, The possibilities of least-squares migration of internally scattered seismic energy: Geophysics, **80**, no. 4, S93-S101.

Dai, W., and G. T. Schuster, 2013, Reverse time migration of prism waves for salt flank delineation: 83rd Annual International Meeting, SEG, Expanded Abstracts, 3861-3865.

Hale, D., N. R. Hill, and J. Stefani, 1992, Imaging salt with turning seismic waves: Geophysics, **57**, no. 11, 1453-1462.

Jin, S., S. Xu, and D. Walraven, 2006, One-return wave equation migration: Imaging of duplex waves: 76th Annual International Meeting, SEG, Expanded Abstracts, 2338-2342.

Li, Y., Y. Agnihotri, and T. Dy, 2011, Prismatic wave imaging with dual flood RTM: 81st Annual International Meeting, SEG, Expanded Abstracts, 3290-3294.

Liu, F., G. Zhang, S. A. Morton, and J. P. Leveille, 2011, An effective imaging condition for reverse-time migration using wavefield decomposition: Geophysics, **76**, no. 1, S29-S39.

Malcolm, A. E., B. Ursin, and V. Maarten, 2009, Seismic imaging and illumination with internal multiples: Geophysical Journal International, **176**, no. 3, 847-864.

Marmalyevskyy, N., Y. Roganov, Z. Gornyak, A. Kostyukevych, and V. Mershchiy, 2005, Migration of duplex waves: 75th Annual International Meeting, SEG, Expanded Abstracts, 2025-2028.

Xu, S., and S. Jin, 2006, Wave equation migration of turning waves: 76th Annual International Meeting, SEG, Expanded Abstracts, 2328-2332.